A Negative Stiffness Dynamic Base Absorber for Seismic Retrofitting of Residential Buildings

Antonios G. Mantakas[1*], Konstantinos A. Kapasakalis[1], Antonios E. Alvertos[2], Ioannis A. Antoniadis[2] and Evangelos J. Sapountzakis[1]

[1] *Institute of Structural Analysis and Antiseismic Research, School of Civil Engineering, National Technical University of Athens, Zografou Campus, GR-157-80 Athens, Greece*

[2] *Dynamics and Structures Laboratory, School of Mechanical Engineering, National Technical University of Athens, Zografou Campus, GR-157-80 Athens, Greece*

Abstract

In this study, a negative stiffness based passive vibration absorber is developed and implemented as a seismic retrofitting measure for typical reinforced concrete (RC) residential buildings. The device, namely the Extended KDamper for Retrofitting (EKD-R), is introduced at the base of the structure, between the foundation level and the first story of the building. The design of the EKD-R device and the selection of its properties are undertaken by incorporating a Harmony Search (HS) algorithm that provides optimized parameters for the mechanism, following constraints and limitations imposed by the examined structural system. Non – linearities due to the plastic behavior of the structural members and soil-structure interaction (SSI) effects are modeled and taken into consideration during the process. Subsequently, a realistic case study of a benchmark 3-story RC building is examined, and the performance of the EKD-R system is assessed. The building superstructure is designed according to Eurocodes. The structure – foundation system, along with the EKD-R, are explicitly modelled using Finite Elements (FE) that may realistically capture structural non-linearities and SSI effects. The HS algorithm is employed, and optimized EKD-R components are obtained and implemented in the benchmark structure. Finally, a series of recorded real ground motions are selected, and non-linear time history dynamic analyses are conducted aiming to assess the behavior of the controlled system. Results indicate the beneficial role of the novel dynamic absorber, hence rendering the concept a compelling seismic retrofitting technology.

Keywords

Dynamic Base Absorber; Seismic Retrofitting; Negative Stiffness; Damping; Earthquake Engineering

1 Introduction & Scope

During the last decades, severe structural damage generated by seismic excitations has motivated extensive research regarding the design of structures, leading to significant alterations of the design codes within the years. Current practice for seismic design relies on increased ductility of structural members and allows substantial inelastic behavior that ensures damping increase and prevention of total collapse. However, permanent drifts and critical loss of functionality of the structure is not avoided in the case of a relatively strong shaking. As a consequence, in order to mitigate the detrimental effects of earthquake motion, seismic isolation has been one of the main approaches

to achieve a robust solution that reduces seismic accelerations and protects the superstructure [1]. Essentially, horizontal isolation is achieved by decoupling the superstructure from its base during shaking and hence, preventing load transfer to the structural members [2].

To this end, a variety of seismic isolation devices have been developed, mainly for applications in bridges and structures of high importance, comprising from simple elastomeric bearings (with and without lead core [3]) to more sophisticated roller bearings and viscous dampers. However, the solution of the base isolation is not panacea and cannot be implemented in every structural application; accelerations are controlled and maintained within reasonable limits but the demand for large base displacements renders this technology inadequate for a number of cases. The overall performance of the structure is affected and provision for flexible utility connections, e.g., waterworks, pipelines, power supplies, that can accommodate large deformations, is required at base level. Furthermore, adequate distance between adjacent structures is essential in order to avoid potential collisions during earthquakes. Implementation to existing structures would require work of high complexity and invasive processes of high cost and risk. As a result of all the above, one of the main drawbacks of base isolation is that its implementation to existing structures, as a means of seismic retrofitting, is almost prohibitive and is rarely considered as a competent option.

Seismic protection advancements focus lately on the development of passive, semi-active, and active vibration control approaches. Among others, these include the incorporation of additional oscillating masses, that introduce damping to the structural system (i.e., Tuned Mass Dampers - TMD), the application of negative stiffness elements (i.e., Negative Stiffness Devices – NS, and Quasi-Zero Stiffness Oscillators - QZS) and TMDs with Inerters (i.e., Tuned Mass Dampers Inerter - TMDI), that could potentially increase the inertial forces of the damper's mass.

The idea of introducing negative stiffness (NS) elements is to assist movement instead of opposing it, as is the case of a positive stiffness element [4]. The pioneering idea of the application of NS in structural systems is to significantly reduce its dynamic stiffness by introducing apparent weakening and thus, decrease its natural frequency [5]. As the isolator's natural frequency is reduced below the predominant energy containing frequencies of seismic motions, its performance is enhanced, and the structure becomes less vulnerable to such vibrations. The effectiveness of the introduction of NS elements has been demonstrated by numerous researchers through numerical, analytical and experimental testing. Such systems include the "Quasi-Zero Stiffness" (QZS) oscillators [6] and NS Devices (NSD) [7–9]. Specifically, in Shen et al. (2017) [10] the analytical procedure from which the optimal parameters of an NS dynamic vibration absorber has been presented. Additionally, Wang et al. (2019) [11] introduced an NS amplifying damper for the seismic protection of SDoF systems and demonstrated the beneficial role of the NS device in the dynamic responses of the uncontrolled structure. For structural systems, the required NS may be achieved using conventional pre-compressed springs arranged in appropriate geometry, post-buckled beams, plates and other pre-stressed mechanical elements [12,13].

The TMD is one of the most popular and well-established approaches to achieve passive vibration control in structures and has been implemented in numerous applications. The concept was first introduced in [14] and comprises an additional mass, a stiffness element and a damper. The TMD system has been adopted in multiple structural applications, such as bridges, skyscrapers [15,16], and in the bases of structures [17–19], aiming to reduce vibration due to ground motion and wind loading. Although the TMD is considered a reliable vibration control method and its applicability has been widely tested, it presents disadvantages that are not negligible: (a) the mass requirements

are significant compared to the total mass of the structure, and (b) environmental factors and material behavior uncertainties may lead to gradual detuning of the system and consequently, to loss of its damping properties and effectiveness [20]. The need for large mass and constructability difficulties, renders its applicability a rather complicated process as a means of seismic retrofitting.

Aiming to overcome the large mass requirement of the above system, various methodologies have been proposed to artificially increase the inertial forces, as in [21]. In Giaralis & Taflanidis (2018) [22] a modification of the TMD has been proposed that includes the addition of an inerter. The so-called Tuned Mass Damper Inerter (TMDI) incorporates an inertance element, which aims to generate an apparent increase of the TMD's inertia, without increasing its actual mass. In various studies [23–25] the TMDI has been implemented as a base absorber supplementary to base isolation, and results indicated improvement of the dynamic behavior of the system as compared to the conventional TMD.

Inspired by the potential of the vibration control systems presented previously, Antoniadis et al. [26] have proposed the KDamper, a novel passive vibration absorption concept based on the optimal combination of appropriate stiffness, mass and damping elements, including a negative stiffness element. The system combines the beneficial characteristics of the NS and of the traditional TMD, leading to a device that introduces extraordinary damping properties to the structure. By incorporating the additional NS element, the inertial forces of the damper are increased and the need for large mass is significantly reduced [27–29]. In addition, the proper allocation of the stiffness – mass elements of the device, leads to a system that is both statically and dynamically stable; the properties of the KDamper can be designed in order to maintain the initial/static stiffness of the structure and hence, avoid potential instabilities. This vibration control system has been examined for the protection of bridges [30,31] wind turbines [32,33], as well as, structural systems [34–36], achieving reduction of the displacement demand at the base level. Specifically, Kapasakalis et al. [34], introduced the extended version of the KDamper concept as a vibration absorber for low-rise buildings; the system was applied supplementary to conventional base isolation for a typical RC structure. Optimization and subsequent analysis were performed by adopting a simplified structural model and by assuming linear structural behavior and linear KDamper components.

In this study, an NS based passive vibration absorber is developed and implemented for the first time in the literature as a seismic retrofitting measure for typical RC residential buildings. The device, namely the Extended KDamper for Retrofitting (EKD-R), is introduced at the base of the structure, between the foundation level and the first story of the building. The design of the EKD-R device, and the selection of its properties, are undertaken by incorporating a Harmony Search (HS) algorithm that provides optimized parameters for the mechanism, following constraints and limitations imposed by the examined structural system. Non – linearities due to the plastic behavior of the structural members and soil-structure interaction (SSI) effects are modeled and taken into consideration during the process. To this end, a number of Eurocode 8 (EC8) compatible artificial seismic motions are generated using SeismoArtif [37], and used as an input to the optimization problem.

Subsequently, a realistic case study of a benchmark 3-story, 1-bay RC building is examined, and the performance of the EKD-R system is assessed. The building superstructure is designed according to the Eurocodes and conventional footings are selected to comply with the EC7, EC8 norms. The structure – foundation system, along with the EKD-R, are explicitly modelled using

Finite Elements (FE) that may realistically capture structural non-linearities and SSI effects. The HS algorithm is implemented, and optimized EKD-R parameters are obtained for the benchmark structure. Finally, a series of recorded ground motions are selected, and non-linear time history dynamic analyses are conducted aiming to assess the behavior of the system. The new system with the EKD-R is compared to the response of the original building and the beneficial role of the retrofitting mechanism in terms of both inter-story drifts and acceleration control is evaluated.

The key features and novelties of the current work can be summarized as follows:

1. For the first time, a novel NS based dynamic absorber is implemented as a retrofitting measure for the seismic protection of buildings, with minimal to no disruption of the existing structure and no need for large parasitic masses that burden the superstructure;
2. Optimization of the EKD-R parameters is undertaken using a set of artificial accelerograms and by employing an HS algorithm that considers the non-linear dynamic behavior of the building, SSI, as well as adaptive NS properties of the NS element specifically designed for the examined structure;
3. For the first time, a more realistic approach is undertaken, and FE analyses are carried out incorporating EKD-R, soil, and structure, using non-linear constitutive models;
4. A benchmark 3-story structure is designed according to European seismic codes (EC8) and the effects of structural non-linearity, SSI, and of a foundation system coupled with this base absorber are examined;
5. The novel, NS based system, is evaluated also by considering real earthquake records, and its superiority to the original system is outlined, hence placing the concept as a compelling seismic retrofitting technology.

2 Methodology & Analytical Model

2.1 Overview of the KDamper Concept as a Passive Dynamic Absorber

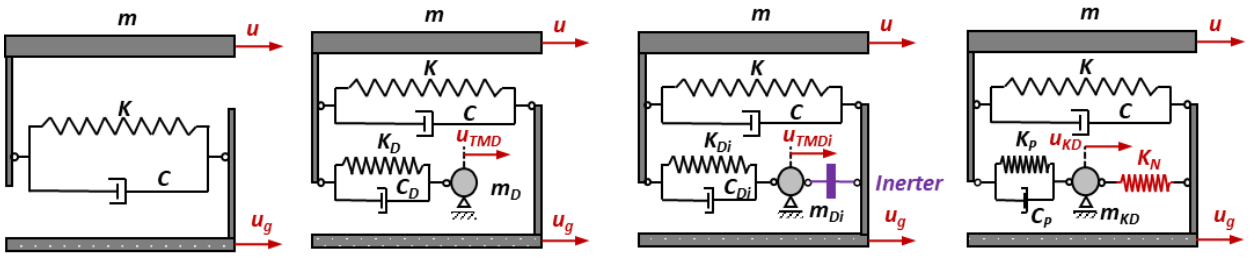

Fig. 1: *a) SDoF oscillator (M-C-K), b) conventional Tuned Mass Damper system (TMD), c) enhanced TMD with grounded inerter (TMDI), d) KDamper concept.*

In this section, the KDamper concept is presented, and the fundamental principles of its function are provided in detail along with the principles of similar isolation systems **(Fig. 1)**. A single degree of freedom (SDoF) oscillator (M-K-C) is considered in which the vibration control system is implemented between its rigid base and the oscillating mass. In a similar approach to the TMD, the KDamper utilizes the additional oscillating mass (m_{KD}) to generate damping and energy

dissipation within the system. However, the KDamper uses an additional NS element K_N, which connects the additional mass to the base. Thus, the equations of motion become:

$$m\ddot{u}_{REL} + c_R\dot{u}_{REL} + Ku_{REL} + c_P\left(\dot{u}_{REL} - \dot{u}_{KD,REL}\right) + K_P\left(u_{REL} - u_{KD,REL}\right) = -m\ddot{u}_G \quad (1.a)$$

$$m_{KD}\ddot{u}_{KD} - c_P\left(\dot{u}_{REL} - \dot{u}_{KD,REL}\right) - K_P\left(u_{REL} - u_{KD,REL}\right) + K_N u_{KD,REL} = -m_{KD}\ddot{u}_G \quad (1.b)$$

were $u_{REL}=u-u_G$, $u_{KD,REL}=u_{KD}-u_G$. The negative stiffness element (K_N) serves as an indirect method to increase the inertial forces of the damper's mass (m_{KD}), as the force of K_N is exactly in phase with the force of m_{KD} [27], without, however, the need to increase the mass itself. The total stiffness of the system with the KDamper can be expressed using the following formula:

$$K + \frac{K_P K_N}{K_P + K_N} = K_0 = (2\pi f_0)^2\left(m + m_{KD}\right) \quad (2)$$

2.2 Implementation of an extended KDamper at Base Level for Seismic Upgrade

In this section, the extended KDamper (EKD) is implemented as a seismic upgrade method for residential buildings. According to Kapasakalis et. al [34] the EKD fundamental principles are identical to that of the KDamper, however its performance is proven to be superior. The EKD is applied between the multi-story superstructure and its base, aiming to control their response to ground motions. For this purpose, the vibration control model is extended from linear SDoF systems (section 2.1) to non-linear MDoF structures. A simplified mathematical model is described in the following subsection, where Soil-Structure-Interaction (SSI) effects are accounted for by using non-linear elements for the soil-foundation-superstructure system.

2.2.1 Simplified Mathematical Model

In this study, the application of the EKD as a seismic protection/Retrofitting measure, which will be referred to hereafter as EKD-R, is examined and implemented at the base of the structure, between the foundation level and the superstructure. The elements of the EKD-R (**Fig. 2**) added for retrofit are the positive stiffness element K_P, the negative stiffness element K_N, and the artificial dampers placed in parallel to these stiffness elements, C_P, and C_N. The corresponding configuration, along with the mathematical model of springs, masses and dampers, is illustrated in **Fig. 2**.

A planar *n*-story building is considered and presented in the sketch of **Fig. 2a**. The following assumptions are made for the modelling of the original uncontrolled structure:

1. the total structure mass is concentrated at floor levels;
2. the slabs and girders on the floors are rigid when compared to the columns;
3. the columns are considered inextensible and weightless, providing the lateral stiffness of the structure;
4. the effect of soil-structure-interaction (SSI) is taken into consideration with the use of non-linear springs coupled in series with the column stiffnesses of the first floor;

5. non-linear behavior of the superstructure is considered by adopting non-linear springs representing the flexural behavior of the columns.

As a result, the original superstructure has *n* dynamic DoFs, represented by the relative to the ground displacements of the *n*-story masses m_j ($j=1, \ldots, n$), as presented in **Fig. 2b**, which are collected in the array $[u_{REL}](t)=[u_{1,REL}(t), u_{2,REL}(t), \ldots, u_{n,REL}(t)]^T$.

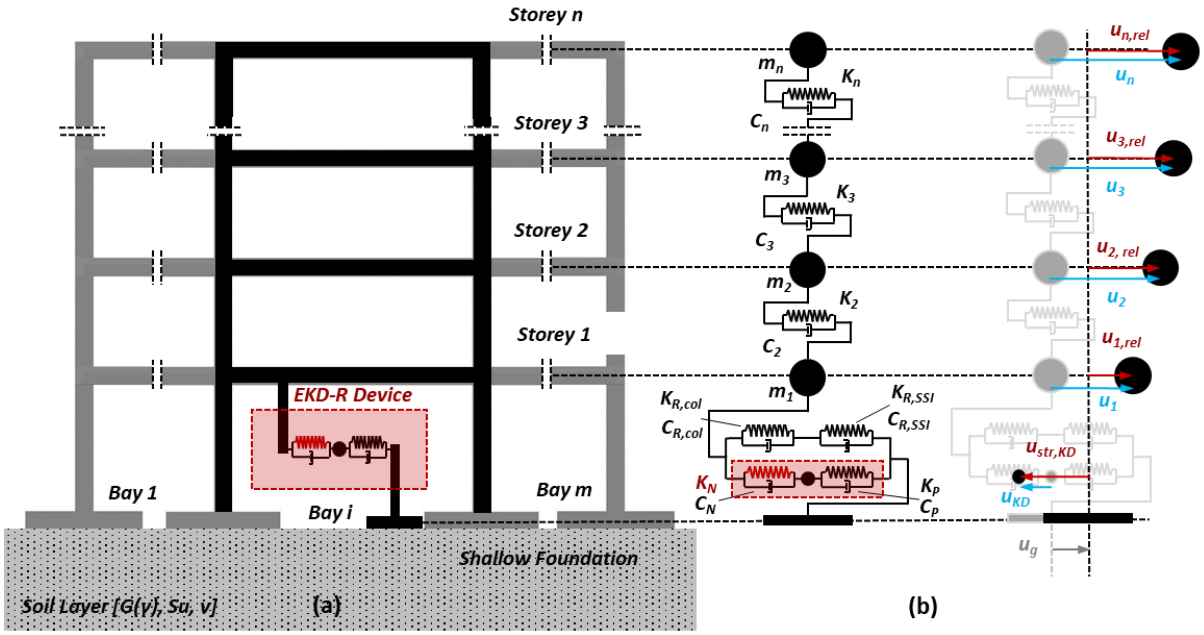

Fig. 2: *a) Schematic presentation of the EKD-R implemented between the foundation and the superstructure (base level of multi-story building), b) Simplified model of the system consisting of masses, non-linear stiffness, and damping elements.*

$K_{R,col}$ represents the non-linear stiffness of the first-floor columns, while $K_{R,SSI}$ the effective horizontal non-linear stiffness (translational and rotational) of the foundation. The equivalent first-floor stiffness K_1 is calculated by coupling the non-linear stiffness of the columns that connect the foundation with the first floor ($K_{R,col}$) along with the non-linear stiffness of the foundation system ($K_{R,SSI}$) that is derived due to the SSI effects, accounting simultaneously for the rotational and translational stiffness of the foundation, as presented in **Fig. 3.** As a result, the total stiffness of the columns-foundations system is calculated as the K_1 of the structure (equivalent 1st floor stiffness), presented in Eq. (3). More details on the derivation of the K_1 and incorporation of the SSI effects are provided in the optimization section (section 3.1) of this paper.

$$K_1(u_{1,REL}) = \frac{K_{R,SSI}(u_G) K_{R,col}(u_{1,REL})}{K_{R,SSI}(u_G) + K_{R,col}(u_{1,REL})} \tag{3}$$

The equations of motion Eqs. (1) still apply, but are now expressed in matrix form, involving matrices with dimensions $r \times r$ with $r=n+1$:

$$[M][\ddot{u}(t)] + [C][\dot{u}(t)] + [K(u)][u(t)] = -[M]1_r^T \ddot{u}_G \tag{4}$$

where the matrices and vectors entering Eq. (4) are defined as:

$$[M]_{r\times r}=\begin{bmatrix}[M_{str}]_{n\times n} & 0\\ 0 & m_{KD}\end{bmatrix} \tag{5.a}$$

$$[K(u)]_{r\times r}=\begin{bmatrix}[K_{str}(u)]_{n\times n} & 0\\ 0 & 0\end{bmatrix}+\begin{bmatrix}[0]_{n-1\times n-1} & [0]_{n-1\times 1} & [0]_{n-1\times 1}\\ [0]_{1\times n-1} & K_N(u_{NS}) & -K_N(u_{NS})\\ [0]_{1\times n-1} & -K_N(u_{NS}) & K_P+K_N(u_{NS})\end{bmatrix} \tag{5.b}$$

$$[C]_{r\times r}=\begin{bmatrix}[C_{str}]_{n\times n} & 0\\ 0 & 0\end{bmatrix}+\begin{bmatrix}[0]_{n-1\times n-1} & [0]_{n-1\times 1} & [0]_{n-1\times 1}\\ [0]_{1\times n-1} & C_N & -C_N\\ [0]_{1\times n-1} & -C_N & C_P+C_N\end{bmatrix} \tag{5.c}$$

$$[u(t)]_{r\times 1}=\begin{bmatrix}[u_{REL}(t)]_{n\times 1}\\ u_{KD}(t)\end{bmatrix} \tag{5.d}$$

where $[M_{str}]_{nxn}$, $[C_{str}]_{nxn}$ and $[K_{str}(u)]_{nxn}$ are the *n*-dimensional matrices of mass, damping and stiffness of the original *n*-story building and $\mathbf{1}_r^T$ is an $n\times 1$ vector of ones (influence vector in the case of horizontal - one dimensional, ground motion). This procedure is serviceable, as it can also be used in the case the *n*-story structure is mounted on a conventional or a highly damped isolation base, as well as any other mass, stiffness, and damping related vibration control system, by properly modifying the matrices in Eqs. (5).

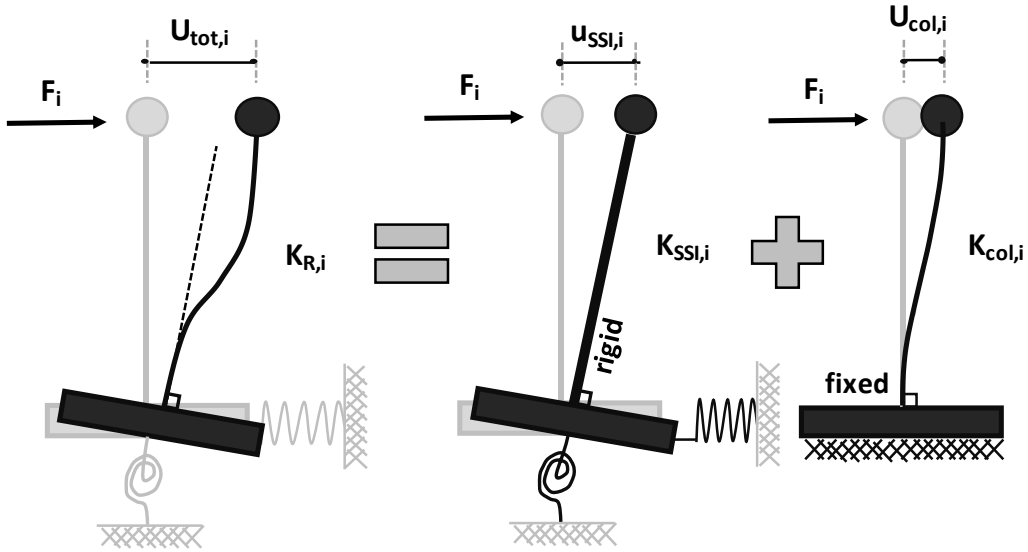

Fig. 3: *Schematic dependencies of K_1 with SSI (horizontal and rotational stiffness of the soil-foundation) and column stiffness for horizontal displacement at the top of the base level columns* [35].

3 Design and Optimization of the EKD-R Parameters

3.1 Optimization parameters

After the equations of motion of the EKD-R and structural system are derived, the aim now is to determine efficient parameters as design variables for the proposed configuration in order to achieve the best possible vibration control strategy. The values of these design variables and the rest of the device parameters are consequently selected with the aid of a constrained optimization process. The objective is to obtain a set of optimal EKD-R parameters that will minimize the relative displacement (drift) of the first floor (critical one), while ensuring that the upper floor accelerations will not exceed a predefined percentage of the peak ground acceleration (filter). For the optimization process, a novel metaheuristic algorithm, the harmony search algorithm (HS), is adopted [38]. Similarly to the genetic algorithms (GA) [39], HS exhibits numerous positive characteristics that render it suitable for various optimization problems. Considering the solution of structural problems with vibration control systems, HS has been employed for the optimum design of the implementation of TMDs to multistory buildings [40,41]. As far as the parameters inherently involved in the HS algorithm are concerned, a common practice is to adopt commonly found values found in relative literature, and are HMS=75, HMCR=0.5, and PAR=0.1.

The objective function and the imposed constraints are selected from the time-domain non-linear dynamic responses. The following are the input parameters to the optimization problem:

1. The mass matrix of the original structure [M_{str}];
2. The horizontal non-linear stiffness parameters of the columns of each floor K_2, …, K_n. More specifically, the stiffness is derived from the moment-curvature relationships that correspond to the reinforced concrete sections of the columns of each floor.
3. The non-linear horizontal base level stiffness of the first floor (K_1). This is implemented in the algorithm as a function of the horizontal displacement of the first floor u_1 and contains both the effect of fist floor column plasticity and of the effect of SSI. In this study, in order to determine the relationship between K_1 and u_1, a pushover analysis has been conducted in a more detailed FE model, provided in the following sections.
4. The additional oscillating mass of the EKD-R: m_{KD}. This is usually expressed as a percentage of the total mass of the structure.
5. The EC8 properties that the original structure design is based on. That is, ground type, spectral peak ground acceleration, spectrum type and importance class.

The non-linear stiffness K_1 is derived from a pushover analysis of the structure in the FE model. This is a simplified, yet widely used approach to model the stiffness of a foundation-soil system and has been extensively studied by various researchers [42,43]. The use of FE analysis is subsequently introduced as a more robust methodology to undertake seismic time-history analyses and evaluate SSI, inertial and kinematic effects in a more realistic manner.

The stiffness parameters of the controlled system (structure + EKD-R) may present significant fluctuations due to numerous reasons, such as temperature variations, manufacturing tolerances, or non-linear behavior of structural elements - that has not been accurately modelled in the mathematical model and in the FE analysis later on - and the unpredictable behavior of the foundation system. Consequently, an increase in the absolute value of K_N and/or a decrease of the

values of K_P and K_1 by a factor ε_N, ε_P, and ε_1, respectively, may result in the system being unstable (the horizontal base level stiffness becomes zero). This situation may happen in the following case:

$$\det\left[K(u)\right]=0 \quad \Rightarrow \quad \left(1-\varepsilon_1\right)K_1(u_1)+\frac{\left(1+\varepsilon_N\right)K_N(u_{NS})\left(1-\varepsilon_P\right)K_P}{\left(1+\varepsilon_N\right)K_N(u_{NS})+\left(1-\varepsilon_P\right)K_P}=0 \tag{6}$$

Assuming that the NS element is realized with pre-compressed springs and is designed to have a symmetric response around its equilibrium position, its maximum absolute value is presented when the system is in static conditions [26,34], as the generated NS decays as the motion proceeds. These assumptions are reasonable, as the necessary elastic forces required to achieve vibration absorption in such structures can be obtained with the aforementioned elements (pre-stressed elastic mechanical elements – springs), and the NS mechanism functions optimally having identical behavior in both ways of the horizontal direction. As a result, if stability is ensured in static conditions (u_1=0 and u_{NS}=0 in Eq. (6)), dynamic stability is certain. Further details regarding the realization of the NS mechanism are presented in section 4.3.

The free design variables taken into consideration in the optimization process are the following:

1. The maximum absolute (initial) value of the negative stiffness element: K_N;
2. The damping coefficients of the viscous dampers employed in the EKD-R: C_P and C_N;
3. The stability factors ε_N, ε_P, and ε_1.

Subsequently, for a specific set of $K_{N,u_{NS}=0}$ and ε_N, ε_P, and ε_1, the value of the positive stiffness element (K_P) of the EKD-R is calculated using Eq. (6).

3.2 Optimization process, constraints and limitations

For the optimal design of the EKD-R, the mathematical model is implemented within a MATLAB script and subsequently analyzed in the time domain. The model is excited with a set of seismic accelerograms that are used as a design and optimization basis. The structure's first floor drift is set as the objective function along with an acceleration filter (AF) that is placed to the acceleration of the upper story, expressed as a percentage of the mean applied PGA.

The proposed control strategy of the EKD-R should be efficient and design values must be selected in a realistic manner. To this end, based on feasibility and technological constraints, appropriate limits are adopted to the free design variables sought in the optimization problem, i.e., K_N , C_N and C_P, as well as the selected value of the additional mass m_{KD} and the stability factors ε_N, ε_P, and ε_R. More specifically:

i. The purpose of this design is to implement a passive vibration absorber at the base of a residential multi-story structure, as a seismic retrofitting measure. Since the EKD-R is implemented at the base, between the foundation and the first story of the building, there are no strict limitations regarding the additional mass. A 0.1% of the total superstructure mass is considered efficient and realistic for the case of this implementation [44].

ii. The NS element, K_N, in the proposed configuration of the EKD-R, is realized with pre-compressed springs. A conceptual design with additional implementation details and constraints is presented in section 4.3 of this study. Based on previous indicative designs

of the EKD concept with pre-compressed springs in [33], the NS element may reach a realistic absolute upper value of -130 *kN/m* per 1 *tn* of total superstructure mass.

iii. The damping coefficient limits should be selected based on the common viscous damping device limitations, available in the market.

iv. The NS element stroke (U_{NS}), namely the absolute relative displacement of the terminals of K_N is set as a constraint with an upper limit of 5 *cm*, based on the details and limitations of the conceptual design presented in section 4.3.

A flow-chart containing the design process as well as the constraints and limitations for a realistic, optimized EKD-R design is depicted in **Fig. 4** below.

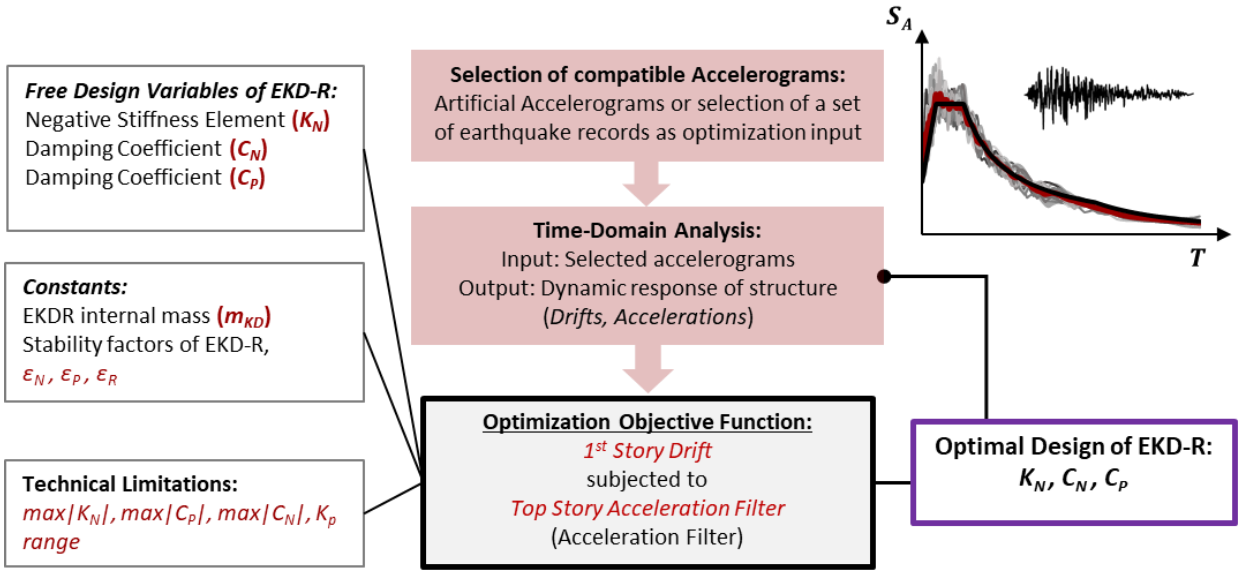

Fig. 4: *Flow-chart briefly presenting the design and optimization process of the EKD-R parameters.*

4 Numerical Test Case

4.1 Benchmark Building Geometry and Characteristics

Aiming to investigate the feasibility and dynamic performance of the EKD-R application on RC buildings, an indicative simplistic structure is employed as a case-study and presented herein. The building consists of a single bay three-story reinforced concrete (C20/25) structure as illustrated in **Fig. 5**. The height of the first story is equal to H_1 =4m while the height of the following floors corresponds to $H_{2,3}$=3m. The building is 6x6m in plan view. The columns are founded on stiff clay of undrained shear strength S_u = 200 kPa and E_o/S_u = 1000 (where E_o is the soil's small-strain elastic modulus), on shallow, rectangular 3x3m foundations.

The structure is dimensioned and reinforced using FESPA design software [45], in accordance with Eurocodes and specifically EC8 for seismic design. For the purposes of this study, the building under consideration is designed assuming the following: ground type C, spectral peak ground acceleration 0.24 g, behavior factor q=3.5, spectrum type I and importance class II. The geometry and structural properties of the RC structure are depicted in **Fig. 5**.

This indicative structure is subsequently adopted as a test case building for the feasibility analysis of the passive seismic control concept using the analytical model (section 2) and non-linear FE numerical analyses (section 4.2).

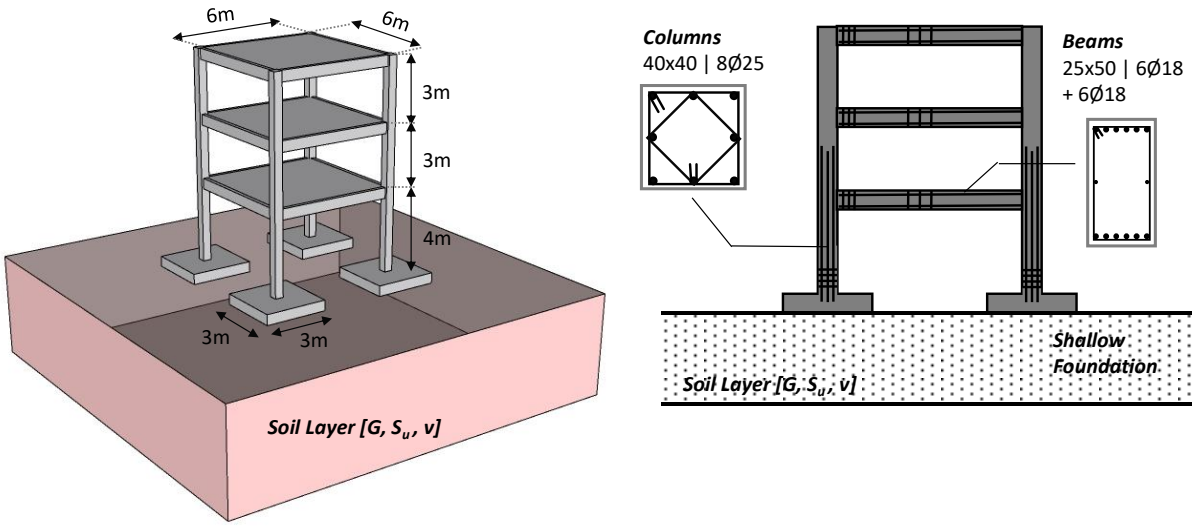

Fig. 5: *Schematic representation of the benchmark structure geometry along with its key structural properties.*

4.2 Numerical (FE) Model

An analysis framework has been developed aiming to calculate reliably the seismic performance of the structural system with and without the EKD-R mechanism. The finite element code ABAQUS [46] was employed for a series of non-linear seismic analyses. The main scope of this more advanced, yet simplified modelling is to capture soil and structural non-linearities and damping effects as well as the soil-structure interaction due to the foundation system of the building. Two-dimensional FE modelling is used to simulate a representative ‘‘slice’’ of the structure and hence realistically capture the soil–foundation interaction effects, while accounting for the appropriate geometry (of soil and superstructure), kinematic boundaries, and foundation response. Inelastic behavior of the soil, foundations and structural elements is modelled explicitly.

More specifically, the soil is modelled with nonlinear plane-strain continuum elements and its stress-strain behavior is described by a nonlinear pressure-dependent kinematic hardening model obeying the Von Mises failure criterion with associative flow rule, proposed by Gerolymos & Gazetas [47] and Anastasopoulos et al [48] for clays under undrained conditions. Despite its simplicity, this constitutive model has been validated against physical model testing, hence ensuring its ability to realistically capture the foundation behavior and the non-linearity of the soil stiffness. The foundation of both the building and the EKD-R is simulated with elastic continuum elements while tensionless contact elements are introduced at the soil-foundation interfaces to model potential uplifting, rocking and sliding. A friction coefficient of $\mu = 0.7$ is applied to the interface between the soil and the footings. Aiming to achieve equivalence between the 2D and the more realistic 3D problem, the Meyerhof [49] and Vesic [50] bearing capacity shape factor of 1.2 (for square foundation) was applied to the out of plane dimension of the soil slice, following the procedure proposed by Gelagoti et al. [51]. This methodology leads to an accurate analogy

between the 2D and the 3D problem in terms of both static and dynamic behavior (stiffness and bearing capacity).

Appropriate "free-field" boundaries are used at the lateral boundaries of the model that are simulated far enough (4 x Bfoot) so as for the reflected seismic waves on them to not intervene with the incident waves, and therefore to not amplify the ground shaking. Dashpots are installed at the base, to simulate the half-space below the 20m of the soil. The damping coefficient is calculated as follows:

$$C_b = \rho V_s A \tag{7}$$

where $\boldsymbol{\rho}$= 2.1 t/m^3 the clay material density, $\boldsymbol{V_s}$ the shear wave velocity corresponding to half-space, and **A** the effective area of each dashpot. In addition, 'node-to node' kinematic constraints are applied along the lateral boundaries of the model (forcing two nodes to have identical displacements). Such approach aims to simulate the response of a plane-strain lateral box subjected to in–plane vertically propagating waves.

The columns and beams of the superstructure are modelled as nonlinear beam elements with moment–curvature (M–C_s) relationship corresponding to the actual reinforced concrete sections (section 4.1), and derived using the RC model of Chang & Mander [52]. Reasonable assumption has been made for the plastic response of RC sections; the residual bending moment capacity (M_{res}) is considered equal to 30% of the ultimate bending moment capacity (M_{ult}) [51]. The moment–curvature behavior of both columns and beams is presented in **Fig. 6** along with the details of the FE model. The density of the structural elements is artificially increased to represent the effective mass acting on the modelled representative soil-structure-foundation "slice"; the mass that acts on the frame should be equal to the 50% of the total mass of the structure. This leads to an accurate representation of the dynamic behavior of the 3-story benchmark symmetric structure, using a 2D FE model.

The EKD-R is modelled by using a point mass element for the internal mass (m_{KD}), a linear spring element acting on the X axis, with a constant stiffness coefficient equal to K_P and a constant damping coefficient equal to C_p. In addition, the model includes a non-linear connector element acting on the X axis, with a variable stiffness coefficient equal to K_N, a constant damping coefficient equal to C_N, and a shallow shaft footing conservatively dimensioned to achieve a rigid foundation for the EKD-R device. The non-linear connector element, K_N, simulates the negative stiffness element and connects the first story beam with the internal mass (m_{KD}) while the linear spring element, K_P, simulates the positive stiffness element and connects the shaft foundation with the internal mass of the device. The damping coefficients are applied to simulate the viscous dampers of the EKD-R. More details on the design of the EKD-R are provided in section 4.3. The dynamic response of the system is simulated by employing nonlinear dynamic time-history analyses, applying the excitation time-history at the base of the model.

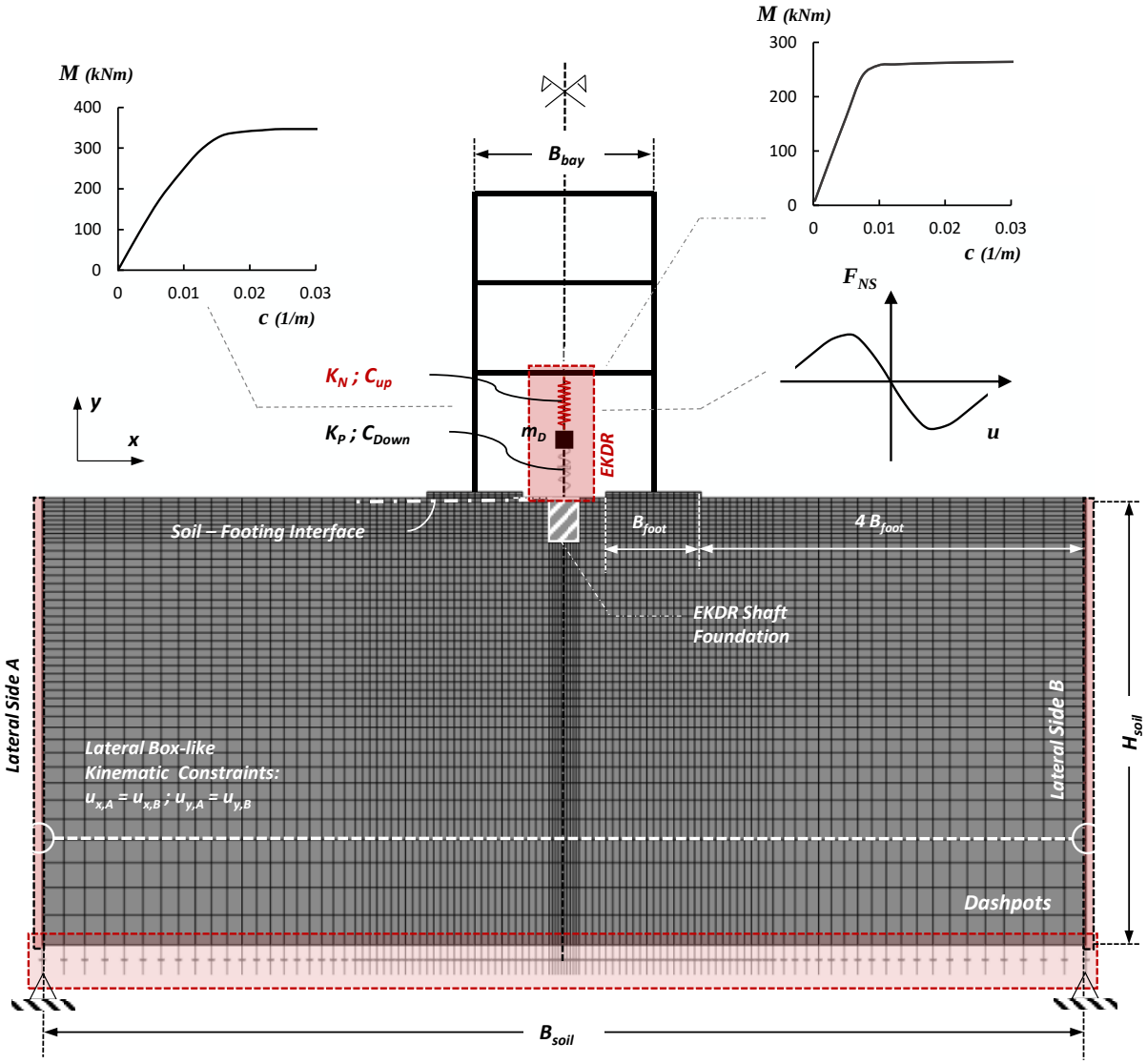

***Fig. 6**: Finite element numerical model and mesh, employed for the dynamic analysis of the benchmark structure. Structural element's non-linear behavior is also presented.*

4.3 Conceptual Design of the Negative Stiffness Device

In order for the EKD-R to be effective in mitigating the seismic effects of earthquakes in building structures, high values of negative stiffness are required. The only feasible option regarding the realization of the negative stiffness elements in such applications is with elastic forces. Among others, special mechanical designs involving conventional positive stiffness pre-stressed elastic mechanical elements, such as post-buckled beams, plates, shells and pre-compressed springs, arranged in appropriate geometrical configurations can generate controlled negative stiffness with the desired magnitude. In this work, the mechanism proposed in [33] is used, and the schematic presentation of this configuration is presented in **Fig. 7**.

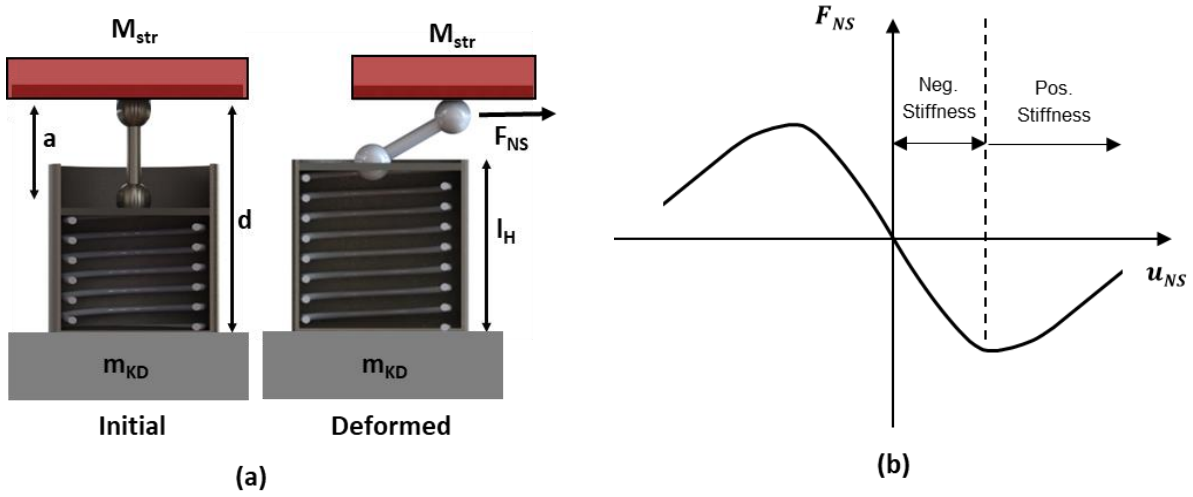

Fig. 7: *a) Conceptual configuration of the NS element, and b) NS force against NS displacement (U_{NS}).*

The following expressions can be derived for the potential energy U, the non-linear force N and the equivalent non-linear stiffness K_N of this mechanism:

$$U(u_{NS}) = \frac{1}{2} k_{spr} \left(l_H - l_{HI} \right)^2 \tag{8}$$

$$N(u_{NS}) = \frac{\partial U}{\partial u_{NS}} = -k_{spr} \left(1 + \frac{l_{HI} - d}{\sqrt{a^2 - u_{NS}^{\ 2}}} \right) u_{NS} \tag{9}$$

$$K_N(u_{NS}) = \frac{\partial N}{\partial u_{NS}} = -K_{spr} \left(1 + \frac{\left(l_{HI} - d \right) / a}{\sqrt[3]{\left(1 - u_{NS}^{\ 2} / a^2 \right)}} \right) \tag{10}$$

where a and d are schematically presented in **Fig. 7**, l_{HI} is the length of the undeformed conventional spring, and K_{spr} is the total stiffness of all the implemented parallel springs.

The generated NS can be easily controlled with Eq. (10) by properly selecting the parameters of this configuration. In previous work of KDamper-based vibration absorption concepts, the generated NS was either assumed constant, or presented a small variation in its absolute value (5-10%). In this work, the generated NS should be carefully designed in order to avoid instability issues, as the coupled stiffness of the first-floor columns with SSI effects decays, as the motion proceeds. For this reason, the generated NS is desired to follow the non-linear horizontal base level stiffness of the first floor. By doing so, the equivalent first-floor stiffness can be maintained in all the range of motion (Eq. (3)). More details are presented in section 4.4.2.

4.4 Selection of the EKD-R Device Parameters

4.4.1 Selection of Seismic Excitations Compatible to the Seismic Design Codes for the Analysis and Optimization of the EKD-R

The optimization problem is formed according to EC8 design response spectrum. Analysis in the time-domain is required for the optimal design of the proposed base absorber. Strong earthquake records can be generated from various types of accelerograms such as synthetic records obtained from seismological models, real earthquake excitations and artificial accelerograms, compatible with a specific design response spectrum [53,54].

For the purposes of this study, a sample of 15 artificial accelerograms is generated using the SeismoArtif [37]. The accelerograms are designed to match the target EC8 response spectra incorporating the following properties: ground type C, spectral acceleration 0.24 g, spectrum type I and importance class II. An exemplar artificial accelerogram is illustrated in **Fig. 8a**, while **Fig. 8b** depicts the acceleration response spectra (Sa) of all the 15 generated records in comparison with the EC8. The mean spectrum of all the records accurately matches the EC8 spectrum.

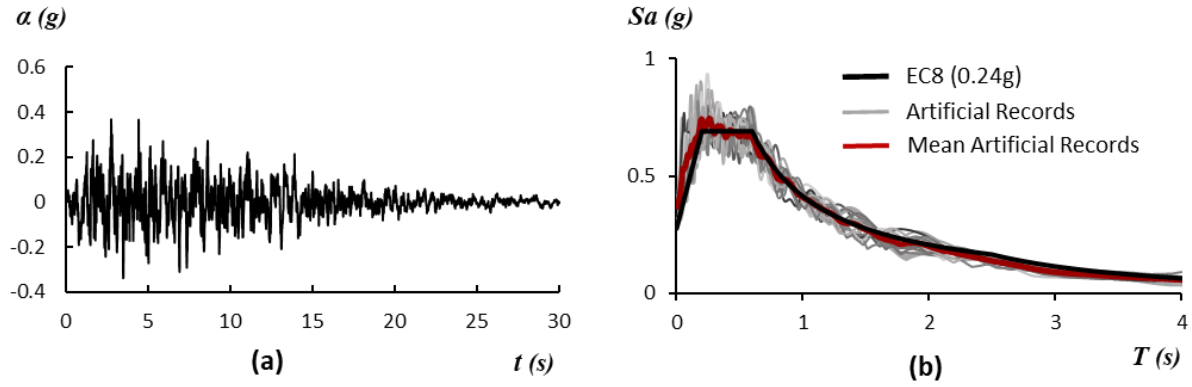

Fig. 8: *a) A typical Artificial Accelerogram generated for the optimization of the EKD-R parameters, and b) the acceleration response spectra of the 15 employed Artificial Accelerograms compared to the EC8 spectrum.*

4.4.2 Optimization Results

The optimization is undertaken using the analytical model and the developed optimization algorithm (section 3). The acceleration filter (AF) imposed in the optimization process is selected equal to 110%, allowing only a 10% increase in the floor absolute accelerations with respect to the mean PGA of the artificial accelerograms. The limits of the free design variables are based on manufacturing constraints. More specifically, based on previous work [34,55], realistic values for the generated NS and the viscous dampers implemented are -130 kN/m and 20 kNs/m per tn of total superstructure mass, respectively. The total superstructure mass of the benchmark building is 36 tn, and thus the limits of the free design variables and the values of the optimized EKD-R components, obtained from the procedure described in section 3, are presented in Table 1. Finally, the additional oscillating mass of the EKD-R is selected to be equal to 0.1% of the total superstructure mass, in order for the realization of the EKD-R device to be feasible and not burden the structure with parasitic masses.

Table 1: *Values of the optimized EKD-R components and limits of the free design variables.*

	m_{KD} *(tn)*	$K_{N\,(uNS=0)}$ *(kN/m)*	C_N *(kNs/m)*	C_P *(kNs/m)*	K_P *(kN/m)*
Limits	0.1%	[-4500 0]	[0 720]	[0 720]	from Eqs. (6)
Design Values	0.31	-3405.4	230.6	22.5	8262.5

The parameters of the NS mechanism are presented in detail in Table 2. Since EKD-R devices can operate in parallel, 4 devices are implemented in total. The proposed configuration presented in section 4.3, is properly designed to match the curve of the first-floor stiffness of the original structure, aiming to maintain the equivalent stiffness of the base level ($K_{1,eq.}$) approximately constant, in all the range of motion. **Fig. 9** presents the equivalent base level stiffness of the original structure along with the one of the controlled structure with the EKD-R.

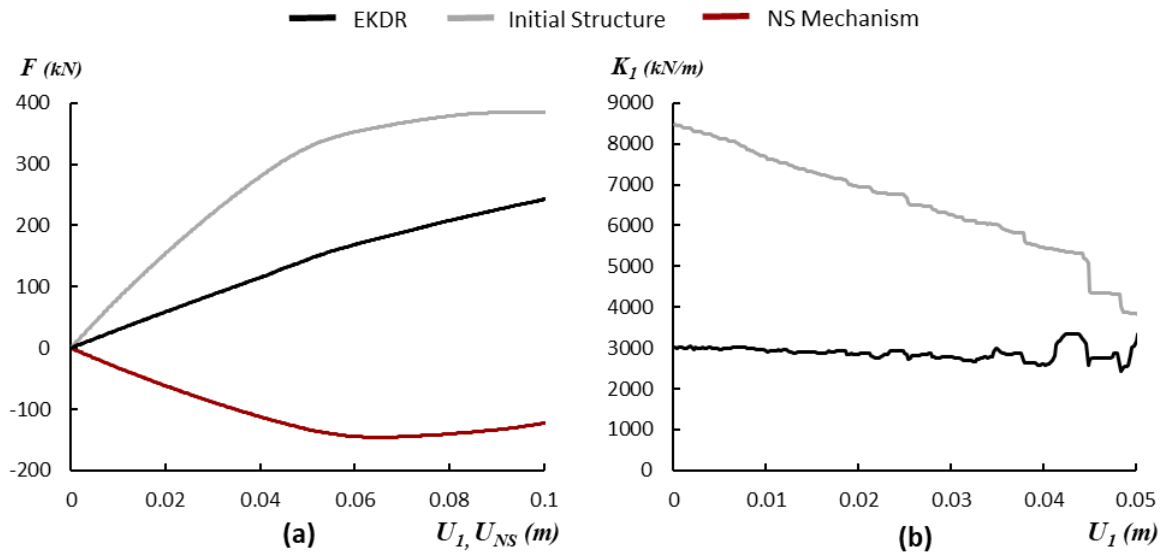

Fig. 9: *a) Force-displacement relationship of the first-story, before and after the application of the EKD-R, and of the designed negative stiffness mechanism, and b) first story stiffness (K_1) – horizontal displacement (u_1) relationship for the system before and after the application of the EKD-R.*

It is observed that the EKD-R manages to sustain the first-floor stiffness effectively within a realistic range of potential U_1 values. Finally, the EKD-R's NS element is schematically presented in **Fig. 10** in its equilibrium position and in the deformed state. The positive stiffness K_{spr} of each EKD-R device is realized with 4 conventional spiral springs (Table 2).

The dynamic response of the original structure, as well as of the controlled system with the EKD-R, for all the generated artificial accelerograms using the analytical model, is summarized in **Fig. 11**. The superstructure's maximum absolute dynamic responses, **Fig. 11a-c**, have been significantly reduced, while at the same time the NS stroke (U_{NS}) is maintained in reasonable ranges, indicating the effectiveness of the optimized parameters.

Table 2: *Negative stiffness mechanism set up parameters.*

K_N (u_{NS}=0) *(kN/m)*	*Kspr (kN/m)*	*Number of devices*	*Number of springs*	*a (m)*	*b (m)*	l_{HI} *(m)*	*d (m)*	*D (m)*	*G (GPa)*
-3405.4	203.63	4	4	0.087	0.253	0.247	0.02	0.1	77

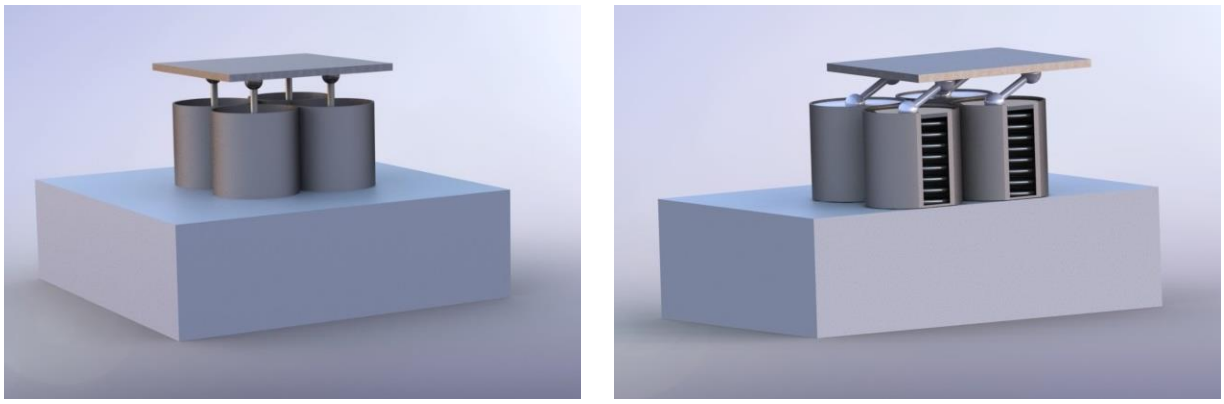

Fig. 10: *Conceptual representation of the realization of the Negative Stiffness elements in the undeformed (left) and deformed state(right).*

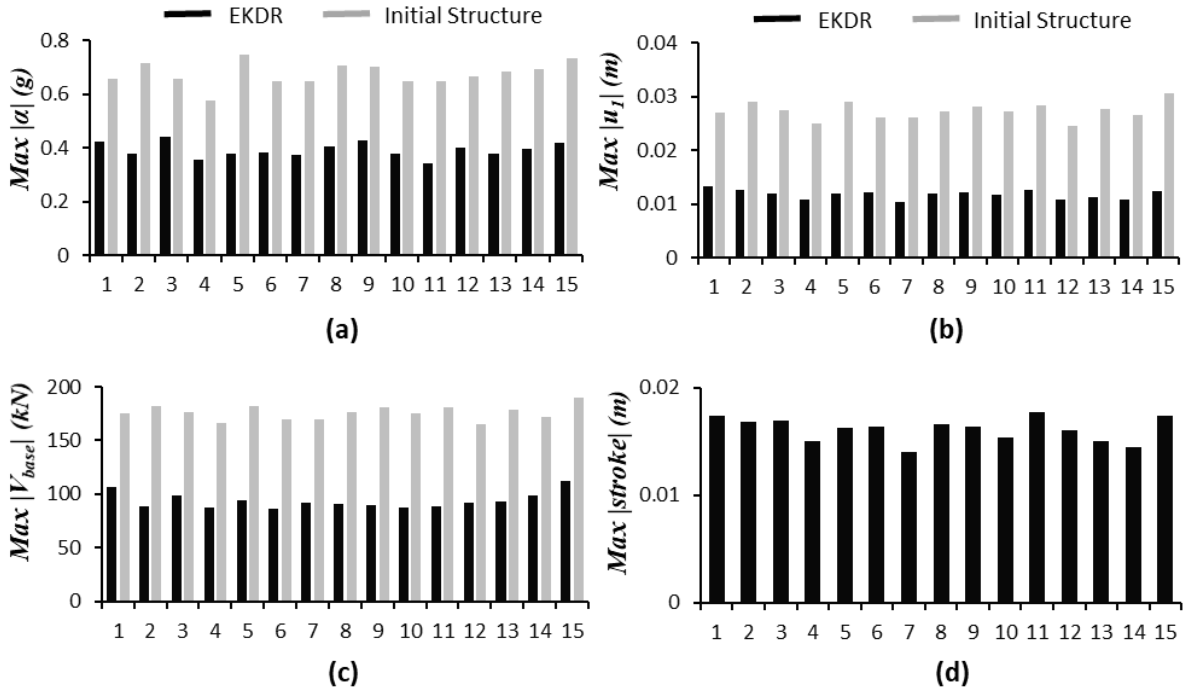

Fig. 11: *Dynamic analysis response of the initial and EKD-R retrofitted system against the 15 EC8 compatible artificial accelerograms, using the analytical model: a) Maximum acceleration of upper story, b) maximum drift values of the 1st story, c) maximum base shear values, and d) maximum relative displacement of the EKD-R mass.*

5 Performance of the EKD-R Against Real Seismic Records

5.1 Selection of Real Ground Motions

Aiming to validate the efficiency of the EKD-R device and examine its dynamic performance, an ensemble of ten (10) recorded real earthquake motions are adopted as input seismic excitation to the benchmark structure. The selected records from the US, European and Asian region cover a wide range and variety of key seismic characteristics such as *PGA*, magnitude *(M_w)*, as well as a broad frequency content, duration and number of significant acceleration cycles. In addition, the employed accelerograms are recorded in stations installed on top of soil formations with shear-wave velocity *($V_{s,30}$)* corresponding to EC8 ground Type C (180-360 *m/s*); this selection ensures that the real records represent realistic earthquake excitations for the assumed benchmark building. Table 3 presents the key characteristics of the selected strong ground motion records.

Table 3: *Characteristics of selected ground records.*

No.	Earthquake	Year	Station	Ground Motion	M_w	PGA *(g)*	R_{jb} *(km)*	DUR *5-75% (s)*
1	Northridge-N	1994	N. Hollywood	Near fault	6.69	0.3087	7.89	7.0
2	Loma Prieta-N	1989	Corralitos	Near fault	6.93	0.6447	0.16	4.6
3	L'Aquila-N	2009	V. Aterno	Near fault	6.3	0.4018	0.0	4.7
4	Chi-Chi-N	1999	CHY006	Near fault	7.62	0.3587	9.76	5.6
5	Kocaeli-N	1999	Izmit	Near fault	7.51	0.1651	3.62	8.2
6	Tabas-N	1978	Tabas	Near fault	7.35	0.8540	1.79	8.3
7	Kobe-N	1995	Amagasaki	Near fault	6.9	0.2758	11.34	6.9
8	Kozani-N	1995	Kozani	Near fault	6.4	0.2069	14.13	3.3
9	Niigata-N	2004	NIG017	Near fault	6.63	0.3781	4.22	6.1
10	Landers-N	1992	Joshua tree	Near fault	7.28	0.2736	11.03	21.7

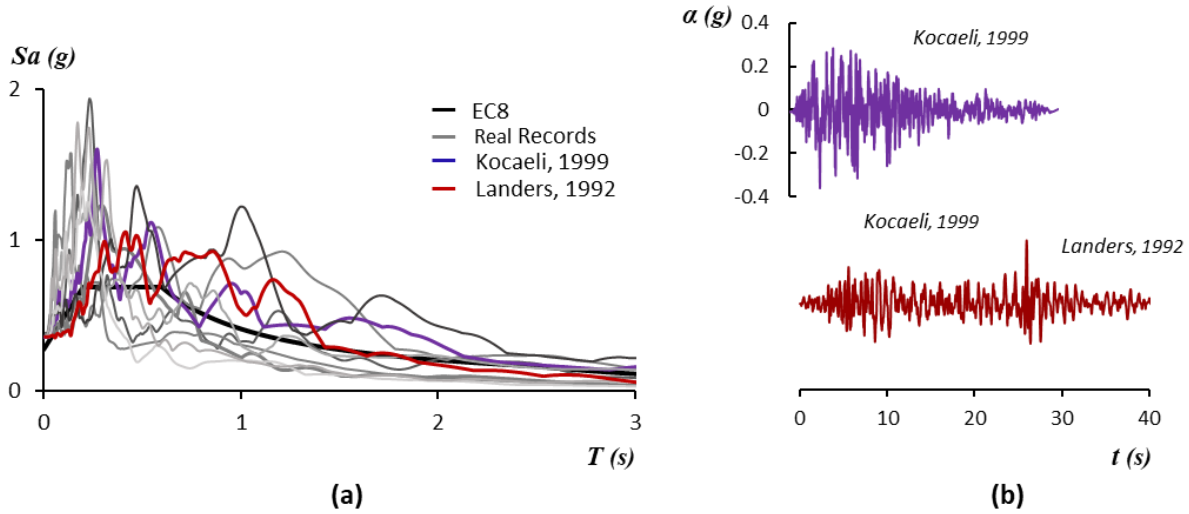

Fig. 12: *a) Acceleration response spectra of all 10 modified ground records along with the EC8 design response spectrum, and b) two (2) characteristic accelerograms, Kocaeli (1999) and Landers (1992) respectively.*

The records are subsequently scaled to a maximum 0.36g *PGA*, aiming to generate acceleration spectra that are above the initial design spectrum of the benchmark structure (EC8-0.24g) and at the same time corresponding to the adopted realistic regional characteristics, assumed for the test case **(Fig. 12)**. Transient time-history analyses are performed using (i) the generated analytical model and (ii) the more sophisticated FE model. A comparison between the performance of the initial structure and the EKD-R upgraded building is subsequently undertaken.

5.2 Time-History Analyses Results

5.2.1 Analytical Model Response

The analytical model's response is presented in terms of maximum 1st story drifts (U_1), upper story accelerations *(a)*, base shear (V_{base}) and EKD-R's NS stroke (U_{NS}). A summary of the building's performance is depicted in **Fig. 13.** Results showcase the superior behavior of the EKD-R retrofitted system in terms of both drifts and accelerations.

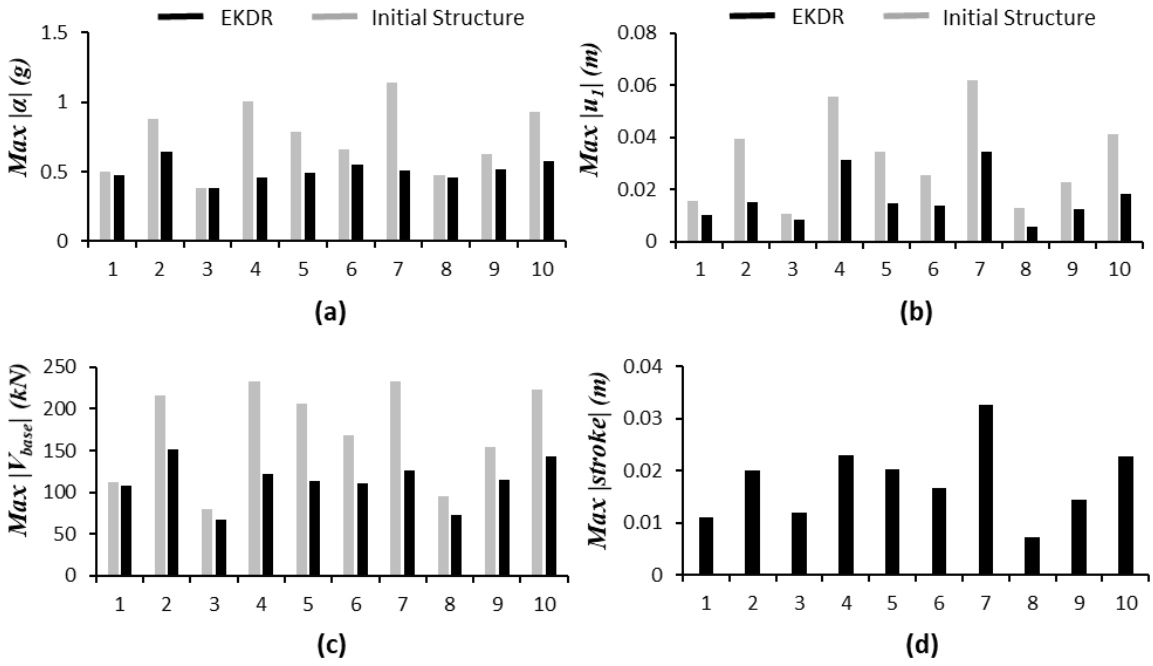

Fig. 13: *Comparative dynamic response results between the initial system and the system with the EKD-R device for all 10 selected real ground records, using the analytical model: a) Maximum acceleration of upper story, b) maximum drift values of the 1st story, c) maximum base shear values, and d) maximum relative displacement of the internal mass of the EKD-R.*

Specifically, the maximum acceleration values are reduced for all earthquake cases with the EKD-R, with an average decrease of 26% and a maximum decrease equal to approximately 56%. A difference in the effectiveness of the EKD-R is observed between the various excitations, as expected due to the variety of seismic motion characteristics (frequency, number of cycles, amplitude, etc.). Nevertheless, the application of the retrofitting device appears to be beneficial for all selected ground motions. As far as maximum drifts are concerned, the EKD-R indicates substantial dynamic performance enhancement, providing 20% to more than 60% reduction of the first story horizontal displacements and an average of approximately 47% reduction for the 10

selected records, as compared to the initial benchmark building. Similar results are obtained for the base shear (V_{base}). Finally, **Fig. 13c** presents the values of the maximum relative displacement of the EKD-R internal mass (U_{NS}). As observed, the maximum U_{NS} value is approximately 3.5 cm, well below the maximum allowed displacements of the designed device (maximum allowed=15cm).

5.2.2 FE Model Response

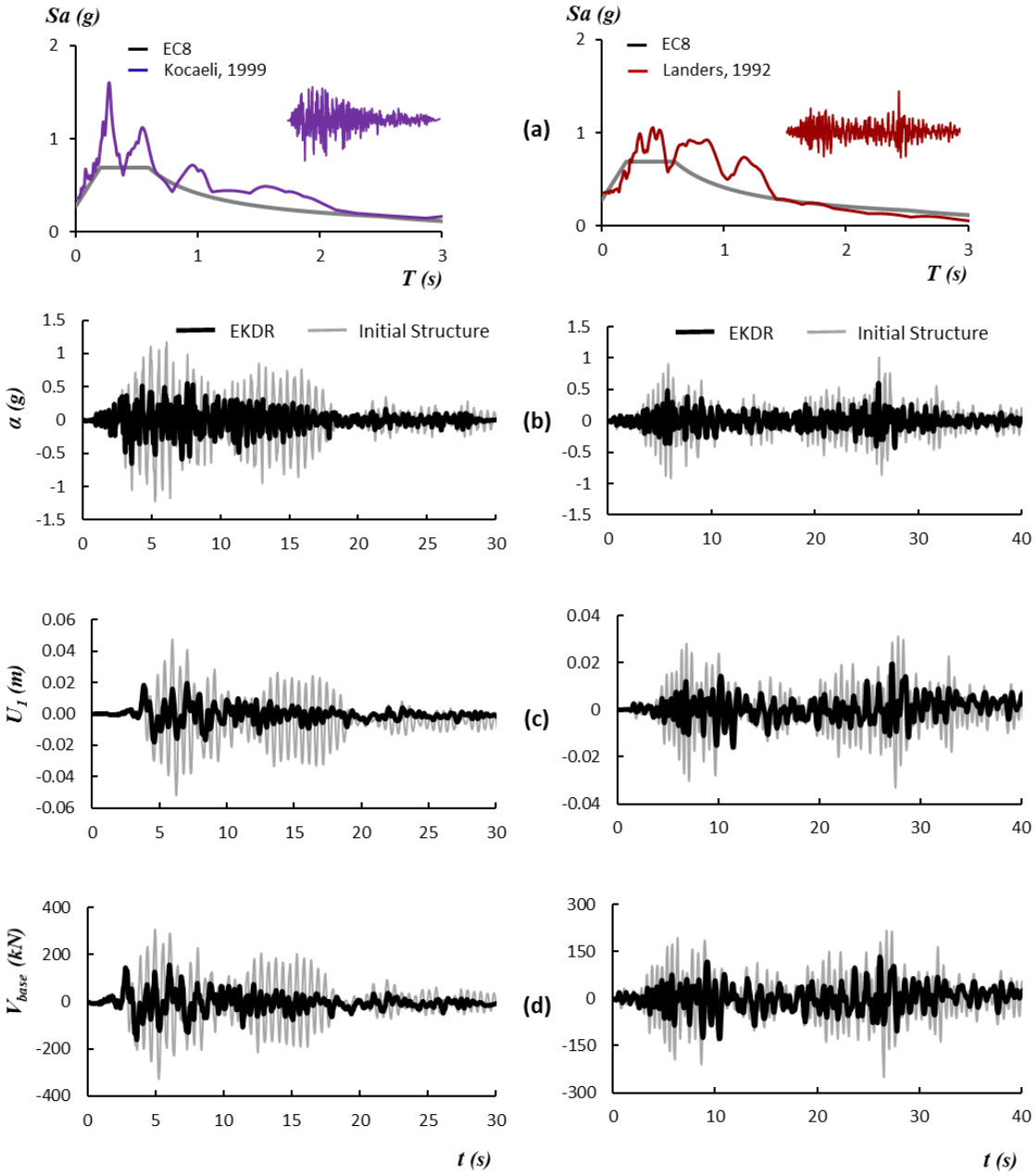

Fig. 14: *Comparative dynamic response results between the initial system and the system with the EKD-R device for the Kocaeli and Landers earthquakes respectively, using the FE model: a) Acceleration response spectra of the two records, b) upper story acceleration, c) first story drift, and d) base shear time histories.*

The dynamic behavior of the RC building columns for both the initial structure and the structure with the EKD-R device is depicted in **Fig. 15**. The plots present the cyclic moment-curvature relationship for the two representative earthquake records. It is observed that for the Kocaeli excitation the initial system exhibits substantial moments, leading to column yielding and non-linear cyclic behavior. On the contrary, the system with the EKD-R remains almost elastic, with no mobilization of its moment capacity. A similar behavior is observed for the case of Landers excitation; this time the initial structure indicates higher moment demand and marginally reaches its yielding point, leading to plastic cyclic behavior. It is clear that for both cases the EKD-R retrofitted structure remains elastic after the excitation while the initial building reaches plasticity that consequently leads to potential column damage.

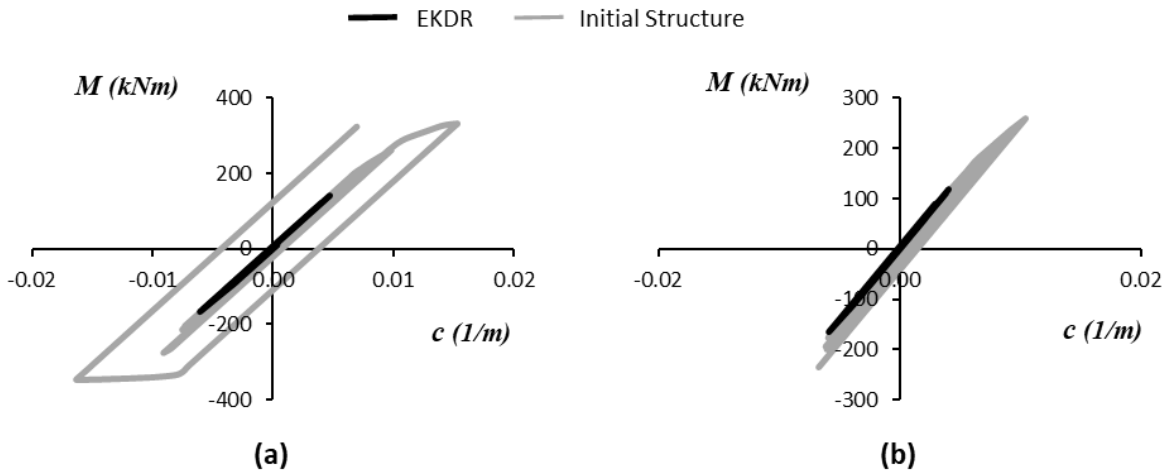

Fig. 15: *Moment-curvature relationship for the initial and EKD-R retrofitted structure for the case of a) Kocaeli (1999), and b) Landers (1992) earthquake records.*

However, for a few of the selected seismic records, even the system with the EKD-R exhibits plastic deformation. An example is the case of the well-known for its detrimental frequency content, Kobe (1995) excitation; dynamic analysis indicated that the system with the EKD-R reaches plastic deformation, however, its behavior is still superior to the initial system. An illustration of the structural behavior of the initial structure and the structure with the EKD-R, for the case of the Kobe (1995) excitation, is presented in ***Fig. 16***. The figure clearly indicates that both systems enter the plastic region; however, the performance of the EKD-R system is superior, showcasing that the system with the EKD-R outperforms the initial structure even for the case of a detrimental shaking that plastic behavior is unavoidable.

Finally, the FE model's response for both the initial and EKD-R retrofitted system is summarized in terms of maximum 1st story drifts (U_1), upper story accelerations *(a)*, base shear (V_{base}) and EKD-R's maximum relative displacement of the internal mass (U_{NS}) in **Fig. 17.**

Results once again indicate the beneficial effect of the EKD-R in terms of both drifts, accelerations, and base shear demand for all 10 selected records. Specifically, the maximum acceleration values are reduced to a minimum of approximately 26% and a maximum decrease equal to approximately 47%. As far as maximum drifts are concerned, the EKD-R provides 30% to more than 60% reduction of the first story horizontal displacements and an average of approximately 44% decrease

for all selected records, compared to the initial benchmark structure. The horizontal displacements of the EKD-R internal mass *(U_{NS})* remain well below the design maximum allowed value (15 cm).

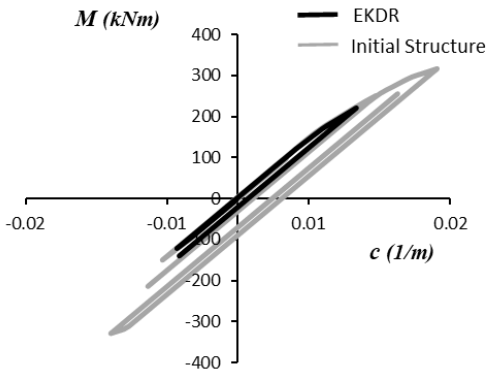

Fig. 16: Moment-curvature relationship for the initial and EKD-R retrofitted structure for the case of the Kobe (1995) earthquake record.

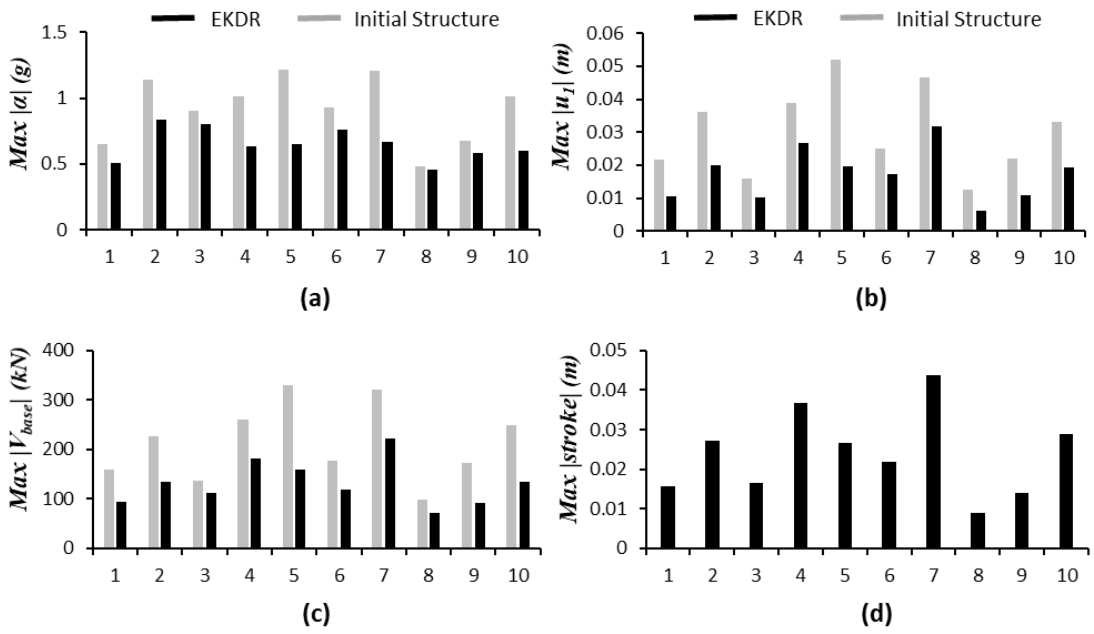

Fig. 17: *Comparative dynamic response results between the initial system and the system with the EKD-R device for all 10 selected real ground records, using the FE model: a) Maximum acceleration of upper story, b) maximum drift values of the 1st story, c) maximum base shear values, and d) maximum relative displacement of the internal mass of the EKD-R.*

5.2.3 Comparison Between the Analytical and FE Model Results

In this final section, a concise summary and comparison between the results of the analytical and numerical (FE) models is presented. **Fig. 18a, b** illustrate the percentage reduction of the maximum top story acceleration values *(a)* and the maximum first story drift values *(U_1)*, after the application of the EKD-R device for all 10 earthquake cases. It is observed that the absolute percentage

reduction for both the analytical and numerical models is similar for most seismic scenarios, hence highlighting the reliability of the analysis. As expected, slight differences between the dynamic response of the two models are observed, especially for the initial system (without the EKD-R mechanism) where soil and structural plasticity are mobilized; the FE model realistically simulates SSI, inelastic cyclic response and hysteretic damping while SSI and hysteresis are not modelled explicitly in the simplified analytical model. However, both models indicate significant improvements of the dynamic behavior of the system. Indicative first story drift and upper story acceleration time-histories for the Kocaeli earthquake scenario, for the case of the EKD-R retrofitted building are plotted in **Fig. 18c, d.** An almost identical dynamic behavior is observed within the time domain between the two models, for this indicative case.

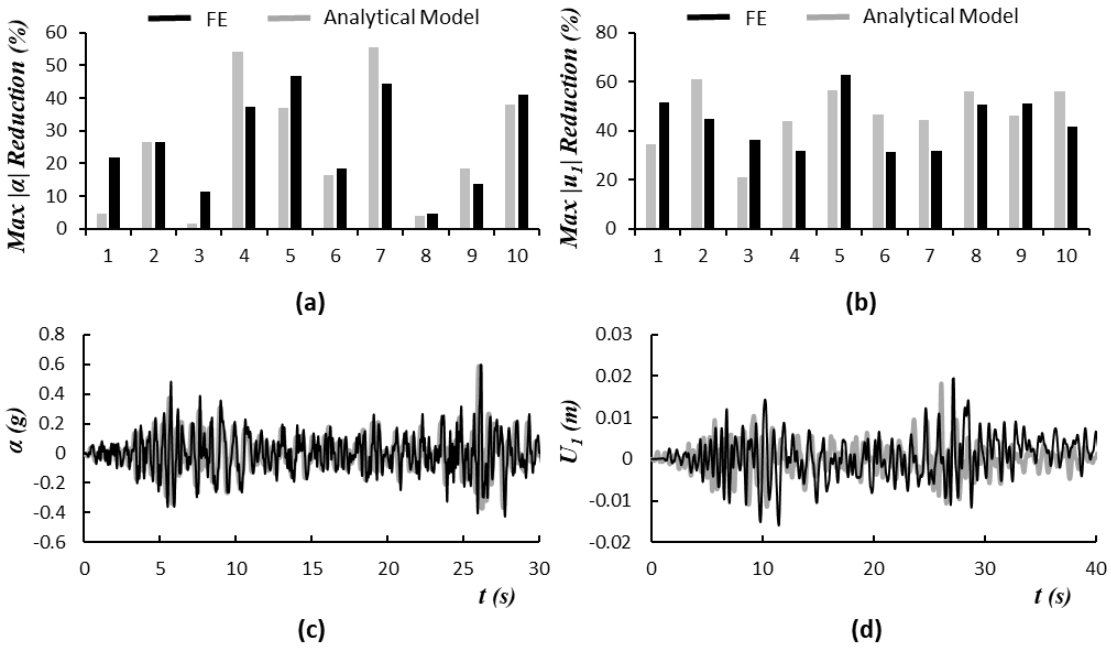

Fig. 18: *Comparative results between the analytical and FE models in terms of a) maximum acceleration reduction, and b) maximum 1st story drift reduction* after the application of the EKD-R to the structure, for all 10 selected real records. Indicative comparison between the FE and analytical time history results for the Kocaeli (1999) record for a) upper story accelerations, and b) 1st story drifts.

6 Summary & Conclusions

This paper investigates the performance of a conventionally designed building structure that incorporates the addition of a novel NS based vibration absorber (EKD-R), as a seismic retrofitting measure. The examined benchmark structure comprises a typical 3-story, one-bay building, designed with the latest European seismic codes (EC8). The research includes structuring of a simplified, non-linear analytical model for the dynamic analysis of the problem, a conceptual design of an adaptive EKD-R mechanism implemented at the base of the structure and optimization of its parameters using a harmony search algorithm. The performance of the benchmark structure under real earthquake excitation, before and after the EKD-R seismic retrofitting, is subsequently examined by employing the simplified analytical model, and more robust numerical (FE) analyses.

More specifically, the study presents an implementation of the EKD-R mechanism at the base of typical residential building structures, between the foundation and the first story. The device comprises an optimal combination of an additional mass, positive and negative stiffness elements as well as damping components. A design and optimization framework of the EKD-R parameters is presented, where non-linearities of the structure, the foundation, and of the NS element are explicitly modelled; the maximum first story drift is set as the objective function of this constrained optimization process.

A benchmark EC8 designed building is subsequently presented, forming a test case for the analysis. A numerical FE model is constructed aiming to realistically capture the dynamic response of the structure. The key structural components (beams, columns) are modelled with non-linear beam elements, while soil and soil-structure interaction are modelled with a suitable inelastic code.

An implementation of the EKD-R for the benchmark test case and conceptual design of the NS element is proposed using pre-stressed spring assemblies and hinged rigid links to connect the NS with the upper structure. The EKD-R design optimization is realized using a set of 15 artificial seismic excitations, compatible with the EC8 design spectrum. The optimization is formed by employing an adaptive/non-linear NS element that follows the stiffness degradation/non-linearity of the RC columns and foundation system in order to maintain the total stiffness of the base (K_1) stable during the motion. Analysis for the 15 artificial records, using the analytical methodology, indicates the beneficial contribution of the optimized EKD-R mechanism to the dynamic performance of the structure; accelerations, drifts and base-shear are significantly reduced.

In the final section, the performance of the EKD-R retrofitted building is investigated under real earthquake records. An ensemble of 10 strong ground motions is employed and applied to both the analytical and FE models. Results indicated the effectiveness of the system as a seismic mitigation measure since both floor accelerations and inter-story drifts were significantly reduced.

The key conclusions derived from the investigation may be summarized as follows:

1. The EKD-R vibration absorber is conceptually designed and implemented as a seismic retrofitting measure that accounts for structural non-linearities as well as SSI effects;
2. A non-linear analytical model has been successfully developed to design and optimize the parameters of the EKD-R with respect to the examined structure and seismic design codes;
3. Analytical and FE numerical analyses on a benchmark building showcased the beneficial effect of the EKD-R on the seismic performance of the structure. Top story accelerations were reduced from approximately 25% to 55% across the selected ground motions while first story drifts from 30% to more than 60%, as compared to the initial system;
4. A comparison between the analytical and FE simulations indicated great similarity between the two. Differences were observed between the dynamic responses of the initial system due to the significance of hysteretic damping, realistic simulation of SSI and kinematic effects captured by the FE. However, the percentage reduction of accelerations and drifts due to the EKD-R application for both models remained in close agreement.
5. Finite element and analytical methods clearly indicated the effectiveness of the EKD-R as a compelling seismic mitigation technology.

Future research foresees examination of the EKD-R performance under two-directional earthquake shaking, as well as experimental validation of the concept using physical testing.

Acknowledgements

Antonios Mantakas would like to acknowledge the financial support provided by the EU's Horizon 2020 research and innovation program under the Marie Sklodowska-Curie grant (Grant Agreement No. INSPIRE-813424, "INSPIRE, Innovative Ground Interface Concepts for Structure Protection"). Konstantinos Kapasakalis would like to acknowledge the support by the Bodossaki Foundation – Scholarship for Postdoctoral studies. The authors would also like to thank Moris Kalderon for his contribution in the illustrations and aesthetics of the paper.

References

[1] Naeim F, Kelly JM. Design of seismic isolated structures: from theory to practice. John Wiley & Sons; 1999.
[2] Symans MD, Charney FA, Whittaker AS, Constantinou MC, Kircher CA, Johnson MW, et al. Energy Dissipation Systems for Seismic Applications: Current Practice and Recent Developments. J Struct Eng 2007;134:3–21. https://doi.org/10.1061/(asce)0733-9445(2008)134:1(3).
[3] Farag M, Mehanny S s. F, Bakhoum M. Establishing optimal gap size for precast beam bridges with a buffer-gap-elastomeric bearings system. Earthquakes Struct 2015;9:195–219. https://doi.org/10.12989/eas.2015.9.1.195.
[4] Molyneaux W. Supports for Vibration Isolation. G. Britain: ARC/CP-322, Aer Res Council; 1957.
[5] Iemura H, Pradono MH. Advances in the development of pseudo-negative-stiffness dampers for seismic response control. Struct Control Heal Monit 2009;16:784–99. https://doi.org/10.1002/stc.345.
[6] Carrella A, Brennan MJ, Waters TP. Static analysis of a passive vibration isolator with quasi-zero-stiffness characteristics. J Sound Vib 2007;301 (3-5):678–89. https://doi.org/10.1016/j.jsv.2006.10.-11.
[7] Sun T, Lai Z, Nagarajaiah S, Li HN. Negative stiffness device for seismic protection of smart base isolated benchmark building. Struct Control Heal Monit 2017. https://doi.org/10.1002/stc.1968.
[8] Sarlis AA, Pasala DTR, Constantinou MC, Reinhorn AM, Nagarajaiah S, Taylor DP. Negative Stiffness Device for Seismic Protection of Structures: Shake Table Testing of a Seismically Isolated Structure. J Struct Eng 2016. https://doi.org/10.1061/(asce)st.1943-541x.0001455.
[9] Pasala DT, Sarlis A, Nagarajaiah S, Reinhorn A, Constantinou M, Taylor D. Adaptive Negative Stiffness: New Structural Modification Approach for Seismic Protection. Adv Mater Res 2013;639–640. https://doi.org/10.4028/www.scientific.net/AMR.639-640.54.
[10] Shen Y, Peng H, Li X, Yang S. Analytically optimal parameters of dynamic vibration absorber with negative stiffness. Mech Syst Signal Process 2017. https://doi.org/10.1016/j.ymssp.2016.08.018.
[11] Wang M, Sun F fei, Yang J qi, Nagarajaiah S. Seismic protection of SDOF systems with a negative stiffness amplifying damper. Eng Struct 2019;190:128–41. https://doi.org/10.1016/J.ENGSTRUCT.2019.03.110.
[12] Winterflood J, Blair D., Slagmolen B. High performance vibration isolation using springs in Euler column buckling mode. Phys Lett A 2002;300:122–30. https://doi.org/10.1016/S0375-9601(02)00258-X.
[13] Virgin LN, Santillan ST, Plaut RH. Vibration isolation using extreme geometric nonlinearity. J Sound Vib 2008;315:721–31. https://doi.org/10.1016/j.jsv.2007.12.025.
[14] Frahm H. Device for damping of bodies. US patent #989958, 1911.
[15] McNamara RJ. Tuned Mass Dampers for Buildings. J Struct Div 1977;103:1785–98.
[16] Qin L, Yan W, Li Y. Design of frictional pendulum TMD and its wind control effectiveness. J Earthq Eng Eng Vib 2009;29:153–7.
[17] Tsai HC. The effect of tuned-mass dampers on the seismic response of base-isolated structures. Int J Solids Struct 1995;32:1195–210. https://doi.org/10.1016/0020-7683(94)00150-U.
[18] Palazzo B, Petti L, de Ligio M. Response of base isolated systems equipped with tuned mass dampers to random excitations. J Struct Control 1997;4:9–22. https://doi.org/10.1002/stc.4300040105.
[19] De Domenico D, Ricciardi G. Earthquake-resilient design of base isolated buildings with TMD at basement: Application to a case study. Soil Dyn Earthq Eng 2018;113:503–21. https://doi.org/10.1016/j.soildyn.2018.06.022.
[20] Weber B, Feltrin G. Assessment of long-term behavior of tuned mass dampers by system identification. Eng Struct 2010;32:3670–82. https://doi.org/10.1016/j.engstruct.2010.08.011.
[21] Kalderon M, Paradeisiotis A, Antoniadis I. 2D Dynamic Directional Amplification (DDA) in Phononic Metamaterials. Materials (Basel) 2021;14. https://doi.org/10.3390/ma14092302.
[22] Giaralis A, Taflanidis AA. Optimal tuned mass-damper-inerter (TMDI) design for seismically excited MDOF structures with model uncertainties based on reliability criteria. Struct Control Heal Monit 2018;25:1–22. https://doi.org/10.1002/stc.2082.
[23] Saitoh M. On the performance of gyro-mass devices for displacement mitigation in base isolation systems. Struct Control Heal Monit 2012;19:246–59. https://doi.org/10.1002/stc.419.
[24] Lazar IF, Neild SA, Wagg DJ. Using an inerter-based device for structural vibration suppression. Earthq Eng Struct Dyn 2014. https://doi.org/10.1002/eqe.2390.
[25] De Domenico D, Ricciardi G. Optimal design and seismic performance of tuned mass damper inerter (TMDI) for

structures with nonlinear base isolation systems. Earthq Eng Struct Dyn 2018;47:2539–60. https://doi.org/10.1002/eqe.3098.
[26] Antoniadis IA, Kanarachos SA, Gryllias K, Sapountzakis IE. KDamping: A stiffness based vibration absorption concept. JVC/Journal Vib Control 2018;24:588–606. https://doi.org/10.1177/1077546316646514.
[27] Kapasakalis KA, Antoniadis IA, Sapountzakis EJ. Performance assessment of the KDamper as a seismic Absorption Base. Struct Control Heal Monit 2020;27. https://doi.org/10.1002/stc.2482.
[28] Paradeisiotis A, Kalderon M, Antoniadis I. Advanced negative stiffness absorber for low-frequency noise insulation of panels. AIP Adv 2021;11:065003. https://doi.org/10.1063/5.0045937.
[29] Andreas P, Moris K, Ioannis A, Lina F. Acoustic performance evaluation of a panel utilizing negative stiffness mounting for low frequency noise control. Proc Int Conf Struct Dyn , EURODYN 2020;2:4093–110. https://doi.org/10.47964/1120.9335.19276.
[30] Sapountzakis EJ, Syrimi PG, Pantazis IA, Antoniadis IA. KDamper concept in seismic isolation of bridges with flexible piers. Eng Struct 2017;153:525–39. https://doi.org/10.1016/j.engstruct.2017.10.044.
[31] Sapountzakis EJ, Syrimi PG, Antoniadis IA. KDamper Concept in Seismic Isolation of Bridges. Proc 1st ICONHIC 2016, Chania, Crete, Greece: 2016, p. 28–30.
[32] Kapasakalis KA, Antoniadis IA, Sapountzakis EJ, Kampitsis AE. Vibration Mitigation of Wind Turbine Towers Using Negative Stiffness Absorbers. J Civ Eng Constr 2021;10:123–39. https://doi.org/10.32732/JCEC.2021.10.3.123.
[33] Kampitsis A, Kapasakalis K, Via-Estrem L. An integrated FEA-CFD simulation of offshore wind turbines with vibration control systems. Eng Struct 2022;254:113859. https://doi.org/10.1016/J.ENGSTRUCT.2022.113859.
[34] Kapasakalis KA, Antoniadis IA, Sapountzakis EJ. Constrained optimal design of seismic base absorbers based on an extended KDamper concept. Eng Struct 2021;226. https://doi.org/10.1016/j.engstruct.2020.111312.
[35] Kapasakalis KA, Alvertos AE, Mantakas AG, Antoniadis IA, Sapountzakis EJ. Advanced negative stiffness vibration absorber coupled with soil-structure interaction for seismic protection of buildings. Proc Int Conf Struct Dyn , EURODYN 2020;2:4160–76. https://doi.org/10.47964/1120.9340.19963.
[36] Kapasakalis KA, Antoniadis IA, Sapountzakis EJ. STIFF vertical seismic absorbers. JVC/Journal Vib Control 2021;0:1–13. https://doi.org/10.1177/10775463211001624.
[37] Seismosoft [2018]. SeismoArtif - A computer program for generating artificial earthquake accelerograms matched to a specific target response spectrum 2018.
[38] Zong Woo Geem, Joong Hoon Kim, Loganathan GV. A New Heuristic Optimization Algorithm: Harmony Search. Simulation 2001;76:60–8. https://doi.org/10.1177/003754970107600201.
[39] Goldberg DE, Holland JH. Genetic Algorithms and Machine Learning. Mach Learn 1988;3:95–9. https://doi.org/10.1023/A:1022602019183.
[40] Nigdeli SM, Bekdaş G, Alhan C. Optimization of seismic isolation systems via harmony search. Eng Optim 2014;46:1553–69. https://doi.org/10.1080/0305215X.2013.854352.
[41] Nigdeli SM, Bekdaş G. Optimum tuned mass damper design in frequency domain for structures. KSCE J Civ Eng 2017;21:912–22. https://doi.org/10.1007/s12205-016-0829-2.
[42] Gazetas G, Anastasopoulos I, Adamidis O, Kontoroupi T. Nonlinear rocking stiffness of foundations. Soil Dyn Earthq Eng 2013;47:83–91. https://doi.org/10.1016/j.soildyn.2012.12.011.
[43] Adamidis O, Gazetas G, Anastasopoulos I, Argyrou C. Equivalent-linear stiffness and damping in rocking of circular and strip foundations. Bull Earthq Eng 2014;12:1177–200. https://doi.org/10.1007/s10518-013-9554-0.
[44] Kapasakalis KA, Antoniadis IA, Sapountzakis EJ. Feasibility Assessment of Stiff Seismic Base Absorbers. J Vib Eng Technol 2021 2021:1–17. https://doi.org/10.1007/S42417-021-00362-2.
[45] Στατικό πρόγραμμα Fespa | LH Λογισμική n.d.
[46] Abaqus Non-Linear FEA Software - The Best Simulation Solver | Simuleon n.d.
[47] Gerolymos N, Gazetas G. Nonlinear lateral response of caisson foundations. Proc. 1st Greece–Japan Work. Seism. Des. Obs. Retrofit Found., 2005, p. 1–24.
[48] Anastasopoulos I, Gelagoti F, Kourkoulis R, Gazetas G. Simplified constitutive model for simulation of cyclic response of shallow foundations: validation against laboratory tests. J Geotech Geoenvironmental Eng 2011;137:1154–68.
[49] Meyerhof G. Some recent research on the bearing capacity of foundations. Can Geotech J 1963.
[50] Vesic AS. Analysis of Ultimate Loads of Shallow Foundations. J Soil Mech Found Div 1973;99:45–73.
[51] Gelagoti F, Kourkoulis R, Anastasopoulos I, Gazetas G. Rocking-isolated frame structures: Margins of safety against toppling collapse and simplified design approach. Soil Dyn Earthq Eng 2012;32:87–102. https://doi.org/10.1016/J.SOILDYN.2011.08.008.
[52] Chang GA, Mander JB. Seismic Energy Based Fatique Damage Analysis of Bridge Columns: Evaluation of Seismic Capacity. National Center for Earthquake Engineering Research; 1994.
[53] Giaralis A, Spanos PD. Derivation of response spectrum compatible non-stationary stochastic processes relying on Monte Carlo-based peak factor estimation. Earthq Struct 2012;3:581–609. https://doi.org/doi: 10.12989/EAS.2012.3.3_4.581.
[54] Cacciola P, D'Amico L. Response-Spectrum-Compatible Ground Motion Processes. Encycl. Earthq. Eng., 2015, p. 1–27. https://doi.org/10.1007/978-3-642-36197-5_325-1.
[55] Kapasakalis K, Antoniadis I, Sapountzakis E. Novel Vibration Absorption Systems with Negative Stiffness Elements for the Seismic Protection of Structures. 4th Natl. Conf. Earthq. Eng. Eng. Seismol. (Hellenic Assoc. Earthq. Eng. - HAEE / ETAM), 2019.